Chapter 4

Comparative Study and Analysis of Newly Designed Squeeze Film Bearing of Different Shapes

Contents

4.1 Introduction

Study of squeeze film behaviour is observed in many fields of real life, for example

1. in industry it is observed in machine tools, gears, rolling elements, hydraulic systems, engines, clutch plates, etc.
2. in human body, it is observed in skeletal joints.

Squeeze film phenomenon arise because of two lubricated surfaces (plates or discs) approach to each other with a normal velocity. This velocity is called squeeze velocity. The authors who have studied this phenomenon from different viewpoints are [10, 22, 32, 53-55, 57, 72, 83, 87, 93, 103, 107].

Agrawal [1] studied effects of ferrofluid (FF) on a porous inclined slider bearing and found that the magnetization of the magnetic particles in the lubricant increases load capacity without affecting the friction on the moving slider. Chi *et. al.* [18] discusses about new type of FF lubricated journal bearing. Sinha *et. al.* [95] discusses about FF lubricated cylindrical rollers with cavitations. Uhlmann *et. al.* [99] discusses about some applications of FFs in tribotechnical systems. Ahmad and Singh [2] studied about FF lubricated porous-pivoted slider bearing with slip velocity. Singh and Gupta [94] studied about curved slider bearing with FF as lubricant. Shah and Bhat [77, 79-82, 84, 86]; Shah [92]; Shah and Patel [89-91]; Shah and Parsania [88] studied about FF lubricated various designed bearings like porous slider bearings of different shapes, long journal bearing, axially undefined journal bearing, squeeze film bearings with the inclusion of effects of slip velocity at the porous boundary and anisotropic permeability of the porous matrix attached to the impermeable plate from different viewpoints.

The purpose of the present study is to analyze and compare newly designed squeeze film bearing of various shapes (exponential, secant and parallel), which formed when a upper porous plate (or disc or surface) approach to a lower one considering the effects of porosity, slip velocity, anisotropic permeability and rotation at both the plates. Moreover, the study also includes the effects of variable porous thickness. The porous matrix (or layer or region) is attached because of its advantageous property of self lubrication. The lubricant used here is water based FF which is controlled by oblique and variable magnetic field. Starting with basic equations from ferrohydrodynamic theory, Reynolds's type equation is derived from which expressions for

pressure and load carrying capacity are obtained. The dimensionless load carrying capacity $\overline{W}$ is calculated for various values of porosity, slip velocity, anisotropic permeability and rotation of both the plates. Moreover, the effects of squeeze velocity and different strength of magnetic field are also considered for the study of $\overline{W}$.

Section 4.2 discusses about the development of mathematical model starting with basic flow equations from ferrohydrodynamic theory. The development is concluded with Reynolds's type equation. Section 4.4 deals with the solution of the Reynolds's type equation derived in section 4.3 with suitable boundary conditions for dimensionless pressure $\bar{p}$ and load carrying capacity $\overline{W}$. Section 4.5 deals with the results and discussion for dimensionless load carrying capacity of the problem and section 4.6 give concluding remarks.

4.2 Mathematical Model of the Problem

Figure 4.1 shows schematic diagram in general of the various bearings under study. It consists of two solid circular plates (upper and lower), each of radius a. The upper plate and lower plate is attached with a porous matrix of thickness l_1 and l_2 respectively. Also, the upper plate moves normally towards lower one with a velocity (known as squeeze velocity) $\dot{h}_0 = dh_0/dt$, where h_0 is central film thickness and t is time. The upper and lower plates are also rotated with angular velocities Ω_u and Ω_l respectively.

As shown in Figure the gap between two porous plates (known as fluid film region or film thickness) is filled with a lubricant and in our case water based FF is used. As FF is controlled by applied magnetic field (Rosensweig [74]), so variable and oblique (to the lower plate) magnetic field **H** with magnitude H of the form

$$H^2 = \frac{Kr^2(a-r)}{a}, \qquad \ldots (4.1)$$

is used for study. Here, K being a quantity chosen to suit the dimensions of both sides of the equation (4.1). K is chosen between 10^{11} to 10^{17} in order to get magnetic field strength between orders of 10^4 to 10^7 and r is radial coordinate.

Three various shapes of film thickness h dependent on the shape of the upper plate are considered for study and are defined as follows:

(a) For exponential pad squeeze film bearing

$$h = h_e = h_0 \exp(-\beta r^2); \quad 0 \le r \le a$$

… (4.2)

(b) For secant pad squeeze film bearing

$$h = h_s = h_0 \sec(\beta r^2); \quad 0 \le r \le a$$

… (4.3)

(c) For parallel pad squeeze film bearing

$$h = h_p = h_0; \quad 0 \le r \le a$$

… (4.4)

where β is the curvature of the upper plate.

In addition to basic flow equations given in (2.11) and (2.12), the velocity of fluid in the film region is

$$\mathbf{q} = u\,\mathbf{i} + v\,\mathbf{j} + w\,\mathbf{k},$$

… (4.5)

where u, v, w are components of film fluid velocity in x, y and z - directions respectively.

The continuity equation of fluid flow for the film region in cylindrical polar coordinates is

$$\frac{1}{r}\frac{\partial}{\partial r}(ru) + \frac{\partial w}{\partial z} = 0,$$

… (4.6)

where r and z are cylindrical polar coordinates, which on integration with respect to z across the film region $(0, h)$ yields

$$\frac{1}{r}\frac{\partial}{\partial r}\int_0^h ru\, dz + w_h - w_0 = 0.$$

… (4.7)

where w_h and w_0 are the values of w at $z = h$ and $z = 0$ respectively.

Basic flow equations for porous region

Considering the validity of the Darcy's law, the velocity components in cylindrical polar coordinates for the fluid flow in upper and lower porous matrix considering rotations of upper and lower plates are given as follows:

For upper porous matrix of width l_1:

$$\bar{u}_1 = -\frac{\psi_r}{\eta}\left[\frac{\partial}{\partial r}\left(P_1 - \frac{1}{2}\mu_0\,\bar{\mu}\,H^2\right) - \rho\, r\, \Omega_u^2\right], (r\text{- direction})$$

… (4.8)

$$\bar{w}_1 = -\frac{\psi_z}{\eta}\frac{\partial}{\partial z}\left(P_1 - \frac{1}{2}\mu_0\,\bar{\mu}\,H^2\right), (z\text{- direction})$$

… (4.9)

where P_1 is the fluid pressure in the upper porous region, ρ is fluid density, μ_0 is free space permeability, $\bar{\mu}$ is magnetic susceptibility and ψ_r, ψ_z are fluid permeabilities in r and z- directions respectively.

For lower porous matrix of width l_2:

$$\bar{u}_2 = -\frac{\varphi_r}{\eta}\left[\frac{\partial}{\partial r}\left(P_2 - \frac{1}{2}\mu_0\,\bar{\mu}\,H^2\right) - \rho\, r\, \Omega_l^2\right], (r\text{- direction})$$

… (4.10)

$$\bar{w}_2 = -\frac{\varphi_z}{\eta}\frac{\partial}{\partial z}\left(P_2 - \frac{1}{2}\mu_0\,\bar{\mu}\,H^2\right), (z\text{- direction})$$

… (4.11)

where P_2 is the fluid pressure in the lower porous region and φ_r, φ_z are fluid permeabilities in *r* and *z*- directions respectively.

The continuity equation of fluid flow in cylindrical polar coordinates for the upper and lower porous matrix are given as follows:

For upper porous matrix of width l_1:

$$\frac{1}{r}\frac{\partial}{\partial r}(r\bar{u}_1) + \frac{\partial \bar{w}_1}{\partial z} = 0.$$

… (4.12)

For lower porous matrix of width l_2:

$$\frac{1}{r}\frac{\partial}{\partial r}(r\bar{u}_2) + \frac{\partial \bar{w}_2}{\partial z} = 0.$$

… (4.13)

4.3 Analysis of the Problem

Combining equations (2.11) to (2.15) using cylindrical polar co-ordinates under an assumption of incompressible, steady, axisymmetric flow and other usual assumptions of lubrication yields equation of motion of fluid in *r*- direction as

$$\frac{\partial^2 u}{\partial z^2} = \frac{1}{\eta}\left[\frac{d}{dr}\left(p - \frac{1}{2}\mu_0\,\bar{\mu}\,H^2\right) - \rho\, r\left(\frac{z}{h}\Omega_r + \Omega_l\right)^2\right],$$

… (4.14)

with

$$\frac{\partial^2 v}{\partial z^2} = 0,$$

… (4.15)

$$\frac{\partial p}{\partial z} = 0,$$

… (4.16)

considering rotation of both upper and lower plates and $\Omega_r = \Omega_u - \Omega_l$, where η is fluid viscosity and p is pressure of fluid in the film region.

Solving equation (4.14) using slip boundary conditions (Shah and Patel [90]; Sparrow *et. al.* [96])

$$u = \frac{1}{s_1}\left(\frac{\partial u}{\partial z}\right) \text{ at } z = 0 \text{ and } u = -\frac{1}{s_2}\left(\frac{\partial u}{\partial z}\right) \text{ at } z = h,$$

… (4.17)

where

$$\frac{1}{s_1} = \frac{\sqrt{\varphi_r \eta_r}}{5} \text{ and } \frac{1}{s_2} = \frac{\sqrt{\psi_r m_r}}{5};$$

… (4.18)

s_1, s_2 are slip parameters, m_r and η_r being the porosity in *r*- direction for upper and lower porous matrix respectively.

One obtains

$$u = \frac{1}{s\eta}\left[\frac{z^2 s}{2}\frac{d}{dr}\left(p - \frac{1}{2}\mu_0 \bar{\mu} H^2\right) - \frac{\rho\, r}{6h^2}\left(\frac{z^4 s}{2}\Omega_r^2 + 2hsz^3\Omega_r\Omega_l + 3sh^2z^2\Omega_l^2\right)\right]$$

$$-\frac{(1+zs_1)}{s\eta}\left[\begin{array}{l}\left(\frac{h^2 s_2}{2} + h\right)\frac{d}{dr}\left(p - \frac{1}{2}\mu_0\bar{\mu}H^2\right) \\ -\frac{\rho\, r}{6h^2}\left\{\left(\frac{h^4 s_2}{2} + 2h^3\right)\Omega_r^2 + (2h^4 s_2 + 6h^3)\Omega_r\Omega_l + (3h^4 s_2 + 6h^3)\Omega_l^2\right\}\end{array}\right],$$

… (4.19)

where

$$s = s_1 + s_2 + hs_1s_2.$$

… (4.20)

Substituting equations (4.8) and (4.9) in the continuity equation (4.12) for upper porous region, yields

$$\frac{\psi_r}{r}\frac{\partial}{\partial r}\left[r\frac{\partial}{\partial r}\left(P_1 - \frac{1}{2}\mu_0\bar{\mu}H^2\right)\right] - 2\rho\,\Omega_u^2\psi_r + \psi_z\frac{\partial^2}{\partial z^2}\left(P_1 - \frac{1}{2}\mu_0\bar{\mu}H^2\right) = 0,$$

… (4.21)

which on integration with respect to z across the upper porous matrix $(h, h + l_1)$, one obtains

$$\psi_z\frac{\partial}{\partial z}\left(P_1 - \frac{1}{2}\mu_0\bar{\mu}H^2\right)\Big|_{z=h} = \frac{\psi_r l_1}{r}\frac{\partial}{\partial r}\left[r\frac{\partial}{\partial r}\left(p - \frac{1}{2}\mu_0\bar{\mu}H^2\right)\right] - 2\rho\,\Omega_u^2\psi_r l_1,$$

… (4.22)

using the fact that the surface $z = h + l_1$ is solid and Morgan-Cameron approximation [67, 81].

Substituting equations (4.10) and (4.11) in the continuity equation (4.13) for lower porous region, yields

$$\frac{\varphi_r}{r}\frac{\partial}{\partial r}\left[r\frac{\partial}{\partial r}\left(P_2 - \frac{1}{2}\mu_0\bar{\mu}H^2\right)\right] - 2\rho\,\Omega_l^2\varphi_r + \varphi_z\frac{\partial^2}{\partial z^2}\left(P_2 - \frac{1}{2}\mu_0\bar{\mu}H^2\right) = 0,$$

… (4.23)

which on integration with respect to z across the lower porous matrix $(-l_2, 0)$, one obtains

$$\varphi_z\frac{\partial}{\partial z}\left(P_2 - \frac{1}{2}\mu_0\bar{\mu}H^2\right)\Big|_{z=0} = -\frac{\varphi_r l_2}{r}\frac{\partial}{\partial r}\left[r\frac{\partial}{\partial r}\left(p - \frac{1}{2}\mu_0\bar{\mu}H^2\right)\right] + 2\rho\,\Omega_l^2\varphi_r l_2\,,$$

… (4.24)

using the fact that the surface $z = -l_2$ is solid and Morgan-Cameron approximation [67, 81].

Assuming that the normal component of velocity across the film-porous interface are continuous, so that

$$w|_{z=h} = w_h = \dot{h}_0 + \bar{w}_1|_{z=h},\ \ w|_{z=0} = w_0 = \bar{w}_2|_{z=0}.$$

… (4.25)

Equation (4.7) using equations (4.19) and (4.25), becomes

$$\frac{1}{r}\frac{\partial}{\partial r}\left\{\frac{r}{s\eta}\left\{\left(-\frac{s_1 s_2 h^4}{4}+\left(\frac{s}{6}-\frac{s_2}{2}-\frac{s_1}{2}\right)h^3-h^2\right)\frac{d}{dr}\left(p-\frac{1}{2}\mu_0\bar{\mu}H^2\right)\right.\right.$$

$$\left.\left.-\frac{\rho\, r}{6h^2}\left[\begin{array}{l}\left(-\frac{s_1 s_2 h^6}{4}+\left(\frac{s}{10}-\frac{s_2}{2}-s_1\right)h^5-2h^4\right)\Omega_u^2\\ +\left(-\frac{s_1 s_2 h^6}{2}-\left(\frac{s}{5}+s_2+s_1\right)h^5+\left(\frac{sh}{2}-2\right)h^4\right)\Omega_u\Omega_l\\ +\left(-\frac{3s_1 s_2 h^6}{4}+\left(\frac{11s}{10}-\frac{3s_2}{2}-s_1\right)h^5-\left(\frac{sh}{2}+2\right)h^4\right)\Omega_l^2\end{array}\right]\right\}\right\}$$

$$+\dot{h}_0\ \ +\bar{w}_1|_{z=h}-\bar{w}_2|_{z=0}=0.$$

… (4.26)

Using equations (4.9), (4.11), (4.22) and (4.24) in the above equation (4.26), yields

$$\frac{1}{r}\frac{\partial}{\partial r}\left[g^*\frac{d}{dr}\left(p-\frac{1}{2}\mu_0\bar{\mu}H^2\right)+f^*\right]=e^*,$$

… (4.27)

where

$$g^*=\frac{r}{s\eta}\left[-\frac{s_1 s_2 h^4}{4}+\left(\frac{s}{6}-\frac{s_1}{2}-\frac{s_2}{2}\right)h^3-h^2\right]-\frac{r}{\eta}\left(\psi_r l_1+\varphi_r l_2\right),$$

$$f^* = -\frac{\rho r^2}{6h^2 s\eta}\left[\begin{array}{l}\left(-\frac{s_1 s_2 h^6}{4}+\left(\frac{s}{10}-\frac{s_2}{2}-s_1\right)h^5-2h^4\right)\Omega_u^2 \\ +\left(-\frac{s_1 s_2 h^6}{2}-\left(\frac{s}{5}+s_2+s_1\right)h^5+\left(\frac{sh}{2}-2\right)h^4\right)\Omega_u\Omega_l \\ +\left(-\frac{3s_1 s_2 h^6}{4}+\left(\frac{11s}{10}-\frac{3s_2}{2}-s_1\right)h^5-\left(\frac{sh}{2}+2\right)h^4\right)\Omega_l^2\end{array}\right],$$

$$e^* = -\dot{h}_0 - \frac{2\rho}{\eta}\left(\psi_r l_1 \Omega_u^2 + \varphi_r l_2 \Omega_l^2\right).$$

Introducing the dimensionless quantities

$$R = \frac{r}{a},\ \ \bar{s}_1 = s_1 h_0,\ \ \bar{s}_2 = s_2 h_0,\ \ \bar{h} = \frac{h}{h_0},\ \ \bar{\psi}_r = \frac{\psi_r}{h_0^2},\ \ \bar{\varphi}_r = \frac{\varphi_r}{h_0^2},$$

$$\Omega_f = \frac{\Omega_l}{\Omega_u},\ \ \bar{l}_1 = \frac{l_1}{h_0},\ \ \bar{l}_2 = \frac{l_2}{h_0},\ \ \bar{p} = -\frac{p h_0^3}{a^2 \eta\, \dot{h}_0},$$

$$S = -\frac{\rho\, \Omega_u^2 h_0^3}{\eta\, \dot{h}_0},\ \ \mu^* = -\frac{K\mu_0 \bar{\mu}\, h_0^3}{\eta\, \dot{h}_0},$$

equation (4.27) reduces to

$$\frac{1}{R}\frac{\partial}{\partial R}\left[RG^*\frac{d}{dR}\left\{\bar{p} - \frac{1}{2}\mu^* R^2(1-R)\right\} + R^2 E^*\right] = 2F^*, \qquad \ldots (4.28)$$

where

$$G^* = \left\{-\frac{\bar{s}_1\bar{s}_2\bar{h}^4}{4} - \left(\frac{2\bar{s}_1 + 2\bar{s}_2 - \bar{s}_1\bar{s}_2\bar{h}}{6}\right)\bar{h}^3 - \bar{h}^2\right\} - \left(\bar{\psi}_r \bar{l}_1 + \bar{\varphi}_r \bar{l}_2\right)\bar{s}\,,$$

$$E^* = -\frac{S}{6}\left[\begin{array}{l}\left\{-\frac{\bar{s}_1\bar{s}_2\bar{h}^4}{4} - \left(\frac{9\bar{s}_1 + 4\bar{s}_2 - \bar{s}_1\bar{s}_2\bar{h}}{10}\right)\bar{h}^3 - 2\bar{h}^2\right\} \\ +\left\{-\frac{\bar{s}_1\bar{s}_2\bar{h}^4}{2} - \left(\frac{6\bar{s}_1 + 6\bar{s}_2 + \bar{s}_1\bar{s}_2\bar{h}}{5}\right)\bar{h}^3 + \left(\frac{\bar{s}_1\bar{h} + \bar{s}_2\bar{h} + \bar{s}_1\bar{s}_2\bar{h}^2 - 4}{2}\right)\bar{h}^2\right\}\Omega_f \\ +\left\{-\frac{3\bar{s}_1\bar{s}_2\bar{h}^4}{4} + \left(\frac{\bar{s}_1 - 4\bar{s}_2 + 11\bar{s}_1\bar{s}_2\bar{h}}{10}\right)\bar{h}^3 - \left(\frac{\bar{s}_1\bar{h} + \bar{s}_2\bar{h} + \bar{s}_1\bar{s}_2\bar{h}^2 + 4}{2}\right)\bar{h}^2\right\}\Omega_f^2\end{array}\right],$$

$$F^* = \frac{\bar{S}}{2}\left[1 - 2S(\overline{\psi}_r \bar{l}_1 + \bar{\varphi}_r \bar{l}_2 \Omega_f^2)\right],$$

which is known as dimensionless form of Reynolds's type equation.

4.4 Solution of the Problem

Solving equation (4.28) under the boundary conditions

$$\bar{p} = 0 \text{ when } R = 1 \text{ and } \frac{d\bar{p}}{dR} = 0 \text{ when } R = 0,$$

yields

$$\bar{p} = \frac{1}{2}\mu^* R^2(1 - R) + \int_1^R \left(\frac{F^* - E^*}{G^*}\right) R \, dR.$$

… (4.29)

The dimensionless form of load carrying capacity W of the bearing is therefore given by

$$\overline{W} = -\frac{W h_0^3}{2\,\pi\, a^4\, \eta\, \dot{h}_0} = \frac{\mu^*}{40} - \frac{1}{2}\int_0^1 \left(\frac{F^* - E^*}{G^*}\right) R^3 \, dR,$$

… (4.30)

where

$$W = 2\pi \int_0^a pr \, dr.$$

… (4.31)

4.5 Results and Discussion

The dimensionless load carrying capacity $\overline{W}$ of the present problem is numerically calculated from equation (4.30) using Simpson's rule with step size 0.1 for the following value of different parameters:

$$a = 0.05(m),\ h_0 = 5.0 \times 10^{-4}(m),\quad \eta_r = 0.64,\quad m_r = 0.81,$$
$$\rho = 1400(Ns^2/m^4),\ \eta = 0.012(Ns/m^2),\ \bar{\mu} = 0.05,$$
$$\mu_0 = 4\pi \times 10^{-7}(N/A^2),\ \Omega_u = 4(rad/s).$$

The calculation of magnetic field strength is shown below:

$$H^2 = \frac{Kr^2(a-r)}{a}$$

$$\text{Max } H^2 = 0.37 \times 10^{-3}K$$

$$\text{For } H = O(10^4),\ K = 10^{11}$$

Moreover, it is assumed in the calculation that $\dot{h}_0 = -V$.

It is clear from equation (4.30) that the increase in the load carrying capacity is the first term of the equation when magnetic fluid (MF) lubricant is used.

The calculated values of $\bar{W}$ for various parameters are shown graphically in Figures 4.2-4.14.

During course of investigation it is noted that the result obtained with respect to l_1 keeping l_2 = 0.000075 fixed as well as with respect to l_2 keeping l_1 = 0.000075 fixed, remains almost same. So, for graphical presentation new parameter L is introduced which implies l_1 (keeping l_2 = 0.000075 fixed) or l_2 (keeping l_1 = 0.000075 fixed).

Figures 4.2-4.4 shows the values of $\bar{W}$ for various values of porous layer width (or thickness) L versus K when β = 4, V = 0.06, $\varphi_r = \psi_r = 10^{-8}$ and Ω_1 = 2 for exponential pad squeeze film bearing (h_e), secant pad squeeze film bearing (h_s) and parallel pad squeeze film bearing (h_p), respectively. It is a general observation that $\bar{W}$ decreases with the increase of width of the porous layer. Moreover, when $0 \le l_2 \le 0.000075$, the rate of decrease of $\bar{W}$ is almost constant (linear and parallel horizontal axis), while when $0.000075 \le l_2 \le 0.0075$, the rate of decrease of $\bar{W}$ is steep. Also, it is a observed that $\bar{W}$ increases with the increase of K; that is, with the increase of strength of magnetic field H. For $K = 10^{15}$, there is a substantial difference in increase of $\bar{W}$.

Figure 4.5 shows the comparative study of $\bar{W}$ for various values of L for h_e, h_s and h_p considering $K = 10^{13}$. It is observed that $\bar{W}$ is more in the case of exponential and parallel pad squeeze film bearings as compared to secant pad. Thus, $\bar{W}_e \geq \bar{W}_p > \bar{W}_s$. Also, it is observed that after 0.0075, all bearings (h_e, h_s and h_p) behaves almost same for $\bar{W}$.

From the above discussion, it is concluded that for smaller values of l_1 and l_2; that is, for smaller thicknesses of l_1 and l_2, $\bar{W}$ is more. It should be noted that smaller thickness implies lower permeability of the porous matrix. In other words, the above conclusion can be stated as $\bar{W}$ is decreasing for higher values of l_1 and l_2. This can be well understood by the following physical process:

According to [96], the pressure of the porous medium provides a path for the fluid to come out easily from the bearing to the environment. The higher the permeability, the more readily does fluid flow through the porous material. In this way, the presence of the porous material decreases the resistance to flow in r- direction and as a consequence the load carrying capacity is reduced. This behavior of decreasing load carrying capacity with the insertion of porous matrix and higher permeability also agrees with the conclusions of Prakash and Tiwari [66] while discussing the problem of squeeze film of rough porous rectangular plates theoretically which was studied experimentally by Wu [107].

Figures 4.6 and 4.7 shows the values of $\bar{W}$ for various values of L versus V when $\beta = 4$, $K = 10^{13}$, $\varphi_r = \psi_r = 10^{-8}$ and $\Omega_l = 2$ for different bearing designs. It is a general observation that $\bar{W}$ increases with the decrease of V. The increase rate is significantly more when $V < 0.0006$. Thus, with the decrease of squeeze velocity, $\bar{W}$ is more effective.

Figures 4.8 and 4.9 shows that $\bar{W}$ increases when β takes values from -8.0 to 8.0; that is, when upper plate takes shape from convex ($\beta < 0$) to concave ($\beta > 0$) for various values of L when $K = 10^{13}$, $V = 0.06$, $\varphi_r = \psi_r = 10^{-8}$ and $\Omega_l = 2$. This behavior agrees with the behaviors of [91].

Figure 4.10 shows the comparative study of $\bar{W}$ when $\beta = 4$ for h_e and h_s. It is observed that $\bar{W}$ increases more in the case of exponential pad squeeze film bearing.

Figures 4.11 and 4.12 shows the results of $\bar{W}$ for various values of φ_r versus ψ_r when $\beta = 4$, $V = 0.06$, $l_1 = l_2 = 0.000075$, $K = 10^{13}$ and $\Omega_l = 2$ for h_e, h_p and h_s, respectively. It is a general observation that $\bar{W}$ decreases with the increase of φ_r. It should be noted here that the decrease rate of $\bar{W}$ is steeper when $\varphi_r > 10^{-9}$. It is also observed that $\bar{W}$ increases with the decrease of ψ_r. Thus, $\bar{W}$ increases for smaller values of permeability parameter. When $\varphi_r > 10^{-6}$ then there is a very little effect on the value of $\bar{W}$. Again, Figures 4.11 and 4.12 it is noted that $\bar{W}$ is more in case of exponential and parallel pad squeeze film bearing.

Figure 4.13 shows the comparative study of $\bar{W}$ for various values of ψ_r when $l_1 = l_2 = 0.000075$, $\beta = 4$, $V = 0.06$, $K = 10^{13}$, $\Omega_l = 2$ and $\varphi_r = 10^{-8}$ for h_e, h_s and h_p. The behavior of the graphs shows that $\bar{W}$ is more in case of exponential and parallel pad squeeze film bearing.

Figure 4.14 shows the comparative study of $\bar{W}$ for various values of Ω_f for $K = 10^{13}$, $\beta = 4$, $V = 0.06$, $l_1 = l_2 = 0.000075$, $\varphi_r = \psi_r = 10^{-8}$ for h_e, h_s and h_p, respectively. It is general observation that $\bar{W}$ is maximum when $\Omega_f = 0$. For positive and negative values of Ω_f, almost symmetrical decreasing behaviour of $\bar{W}$ is obtained; that is, $\Omega_f = 0$ line is mean line. Again, it is observed that $\bar{W}$ more in case of h_e and h_p.

Percentage increase in $\bar{W}$

Effect on $\bar{W}$ for different bearing designs

The following numerical value of $\bar{W}$ for different bearing designs is obtained when $l_1 = 0.000075$, $l_2 = 0.0000075$, $\beta = 4$, $V = 0.06$, $\varphi_r = \psi_r = 10^{-8}$, $\Omega_l = 2$ and $K = 10^{13}$.

Bearing designs	For exponential pad squeeze film bearing (h_e)	For secant pad squeeze film bearing (h_s)	For parallel pad squeeze film bearing (h_p)
$\bar{W}$	0.5974	0.1727	0.5869
% increases in $\bar{W}$ as compared to h_s	245.92	100	239.84

It is observed from the above table that $\bar{W}$ increases on average 243 % for exponential and parallel pad squeeze film bearing as compared to secant pad.

Effect of FF on different bearing designs

The following numerical value of $\bar{W}$ for different bearing designs is obtained when $l_1 = 0.000075$, $l_2 = 0.0000075$, $\beta = 4$, $V = 0.06$, $\varphi_r = \psi_r = 10^{-8}$ and $\Omega_l = 2$.

K	0.0 (Using Conventional Lubricant or Without using FF lubricant)			1.0E+15 (Using FF Lubricant)			% increases in $\bar{W}$ because of FF as lubricant		
Bearing designs	h_e	h_s	h_p	h_e	h_s	h_p	h_e	h_s	h_p
$\bar{W}$	0.5947	0.1700	0.5842	0.8675	0.4428	0.8570	45.87	160.47	46.70

It is observed that because of using FF as lubricant $\bar{W}$ increases approximately 46% for exponential and parallel pad squeeze film bearing whereas it will increase approximately 160% for secant pad squeeze film bearing. Thus, secant pad squeeze film bearing affected more when FF considered as lubricant.

Effect of squeeze velocity on different bearing designs

The following numerical value of $\bar{W}$ for different bearing designs is obtained when $l_1 = 0.000075$, $l_2 = 0.0000075$, $\beta = 4$, $K = 10^{13}$, $\varphi_r = \psi_r = 10^{-8}$ and $\Omega_l = 2$.

V	0.06			0.00006			% increases in $\bar{W}$		
Bearing designs	h_e	h_s	h_p	h_e	h_s	h_p	h_e	h_s	h_p
$\bar{W}$	0.5974	0.1727	0.5869	3.0315	2.6150	3.0213	407.45	1414.19	414.79

It is observed that because of using smaller values of V (that is, when small squeeze velocity), $\bar{W}$ increases approximately 410 % for exponential and parallel pad squeeze film bearing whereas it will increase approximately 1414% for secant pad squeeze film bearing. Thus, secant pad squeeze film bearing affected more by V.

Effect of curvature on different bearing designs

The following numerical value of $\bar{W}$ for different bearing designs is obtained when $l_1 = 0.000075$, $l_2 = 0.0000075$, $V = 0.06$, $K = 10^{13}$, $\varphi_r = \psi_r = 10^{-8}$ and $\Omega_l = 2$.

β	-8.0		8.0		% increases in $\bar{W}$	
Bearing designs	h_e	h_s	h_e	h_s	h_e	h_s
$\bar{W}$	0.5667	0.1667	0.6080	0.1748	7.29	4.86

It is observed that when the upper plate is concave ($\beta > 0$), $\bar{W}$ for exponential pad squeeze film bearing increases approximately 7.0 % whereas for secant pad squeeze film bearing it will increases approximately 5.0%.

Effect of φ_r on different bearing designs

The following numerical value of $\bar{W}$ for different bearing designs is obtained when $l_1 = l_2 = 0.000075$, $\beta = 4$, $V = 0.06$, $K = 10^{13}$, $\Omega_l = 2$ and $\psi_r = 10^{-8}$.

φ_r	10^{-6}			10^{-11}			% increases in $\bar{W}$		
Bearing designs	h_e	h_s	h_p	h_e	h_s	h_p	h_e	h_s	h_p
$\bar{W}$	0.0847	0.0585	0.0844	0.6499	0.1825	0.6382	667.30	211.96	656.16

It is observed that with the decrease of permeability φ_r from 10^{-6} to 10^{-11}, $\bar{W}$ increases approximately 667 % for exponential squeeze film bearing, 212 % for secant pad squeeze film bearing, and 656% for parallel pad squeeze film bearing.

Effect of ψ_r on different bearing designs

The following numerical value of $\bar{W}$ for different bearing designs is obtained when $l_1 = l_2 = 0.000075$, $\beta = 4$, $V = 0.06$, $K = 10^{13}$, $\Omega_l = 2$ and $\varphi_r = 10^{-8}$.

ψ_r	10^{-6}			10^{-11}			% increases in $\bar{W}$		
Bearing designs	h_e	h_s	h_p	h_e	h_s	h_p	h_e	h_s	h_p
$\bar{W}$	0.0840	0.0576	0.0837	0.6560	0.1837	0.6442	680.95	218.92	669.65

It is observed that with the decrease of permeability ψ_r from 10^{-6} to 10^{-11}, $\bar{W}$ increases approximately 681 % for exponential squeeze film bearing, 219 % for secant pad squeeze film bearings, and 670% for parallel pad squeeze film bearing.

4.6 Conclusion

The problem of newly designed squeeze film bearing of various shapes (exponential, secant and parallel) considering the effects of porosity, slip velocity, anisotropic permeability and rotation at both the plates is discussed here for its optimum performance in the sense of efficient and durable bearing because production of efficient and durable bearings always has an attraction for Industry. The porous layered attached at both the plates because of its advantages property of self lubrication. The problem also includes the effects of study of variable porous thickness for both the plates. The lubricant used here water based FF which is controlled by oblique and variable magnetic field. The following conclusions can be made in order to increase the efficiency and durability of bearings.

$\bar{W}$ can be increased

(1) when width of upper porous layer decreases.

(2) when width of lower porous layer decreases.

(3) when taking higher value of K ($K \geq 10^{14}$); that is, the magnetic field strength is of the order grater than or equal to 10^5.

(4) with the decreasing values of squeeze velocity V.

(5) with the decreasing values of permeabilities φ_r and ψ_r.

(6) for small rotations of the upper plate.

From the result and discussion, the best bearing design for the considering bearing problem can be obtained when $l_1 = l_2 = 0.000075$, $O(H) \geq 10^5$, $\varphi_r = \psi_r = 10^{-9}$ and $\beta = 8$ for concave upper plate. Moreover, for exponential pad squeeze film bearing $\bar{W}_e$, parallel pad squeeze film bearing $\bar{W}_p$ and secant pad squeeze film bearing $\bar{W}_s$, the behaviour with respect to increase of $\bar{W}$ can be obtained as $\bar{W}_e > \bar{W}_p > \bar{W}_s$.

During the course of investigating it is observed from equation (4.14) that Rosensweig's model of FF does not affect on the performance of the bearing system when uniform magnetic field is used.

4.7 Figures

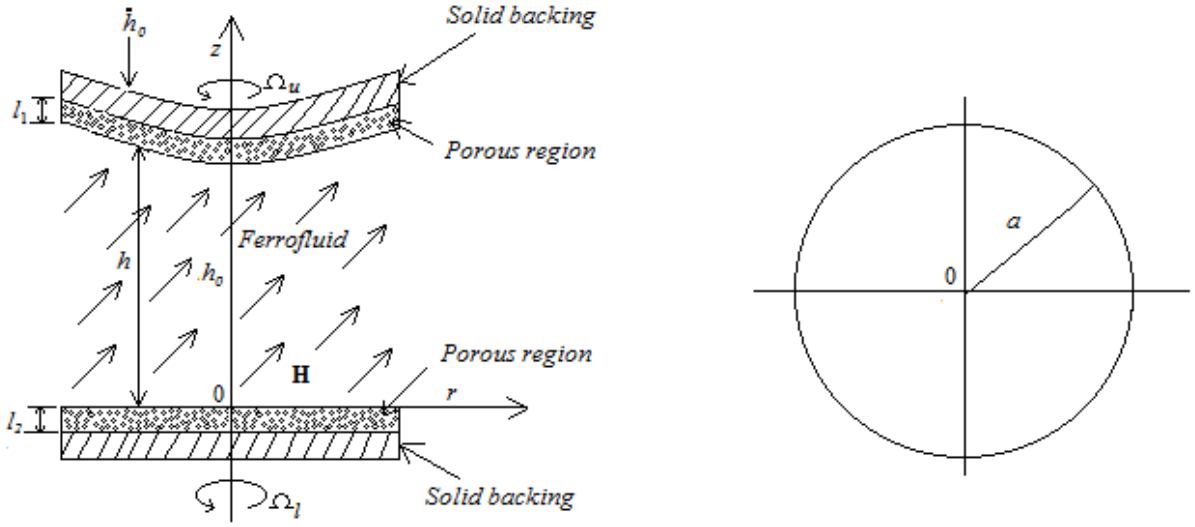

Front view Top view

Figure 4.1 Schematic diagram of squeeze film bearing configuration

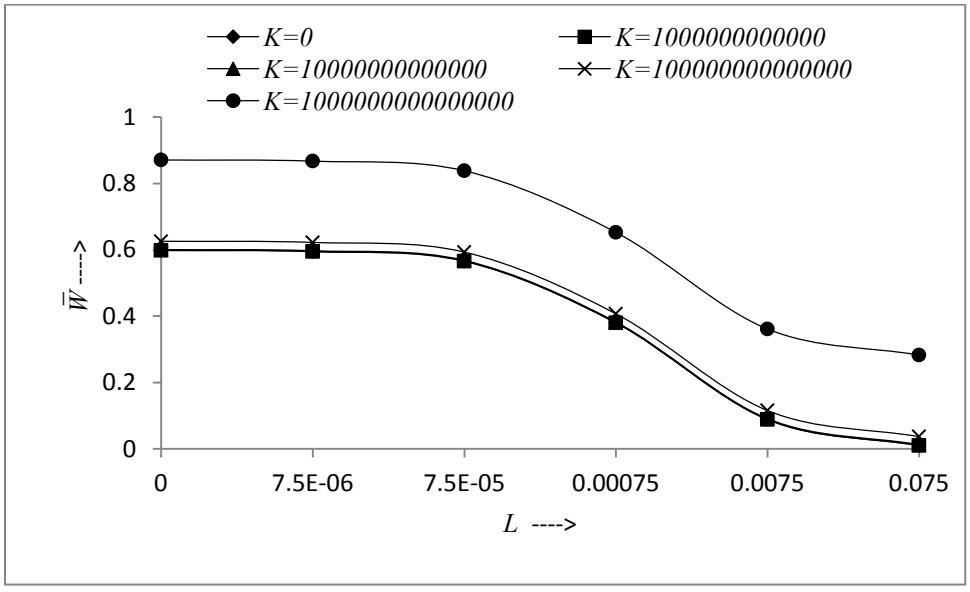

Figure 4.2 Values of $\bar{W}$ for various values of L versus K when $\beta = 4$, $V = 0.06$, $\varphi_r = \psi_r = 10^{-8}$ and $\Omega_l = 2$ for h_e

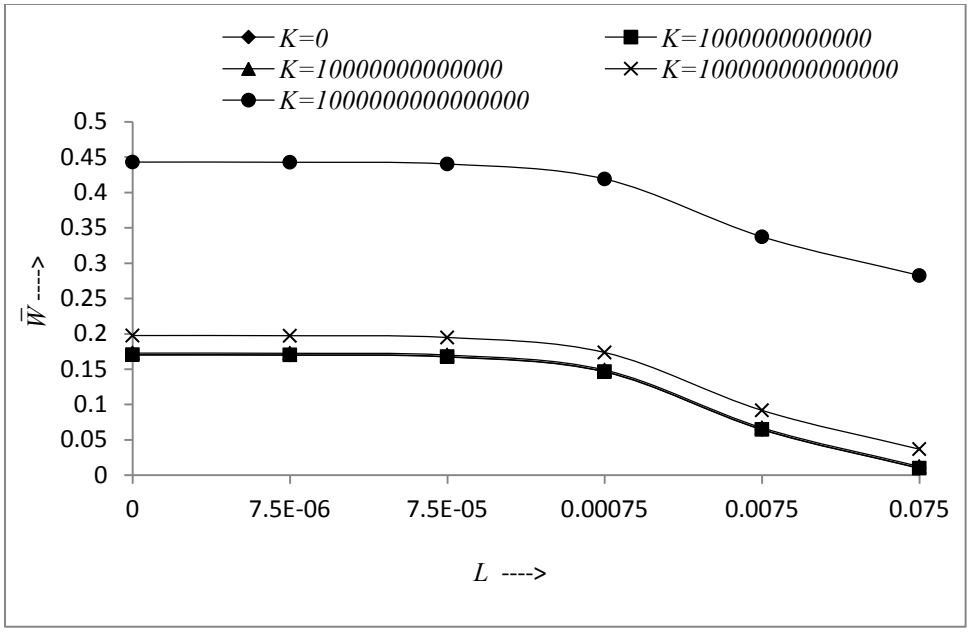

Figure 4.3 Values of $\bar{W}$ for various values of L versus K when $\beta = 4$, $V = 0.06$, $\varphi_r = \psi_r = 10^{-8}$ and $\Omega_l = 2$ for h_s

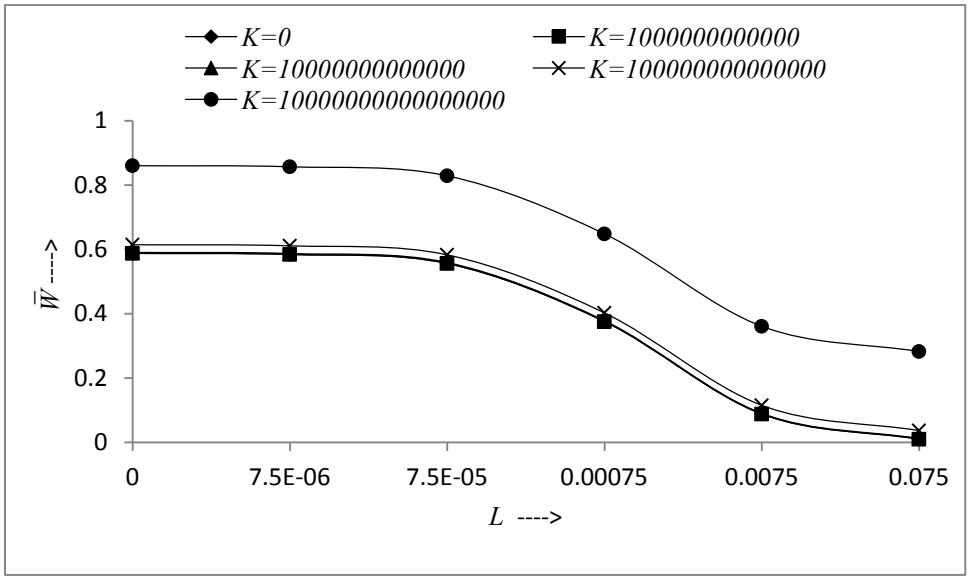

Figure 4.4 Values of $\bar{W}$ for various values of L versus K when $\beta = 4$, $V = 0.06$, $\varphi_r = \psi_r = 10^{-8}$ and $\Omega_l = 2$ for h_p

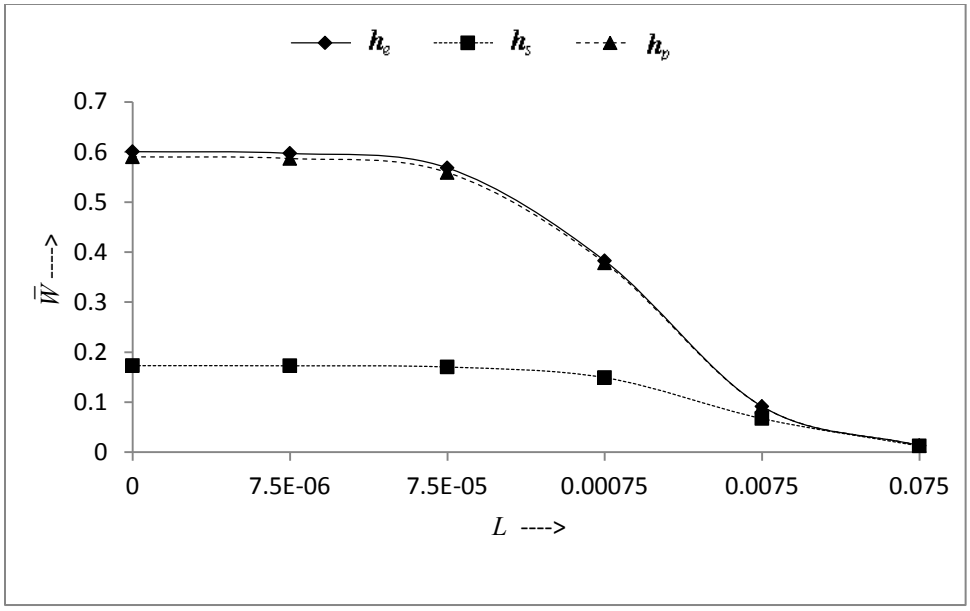

Figure 4.5 Comparative study of $\bar{W}$ for various values of $L$when $\beta = 4$, $V = 0.06$, $\varphi_r = \psi_r = 10^{-8}$, $\Omega_l = 2$ and $K = 10^{13}$ for h_e, h_s and h_p

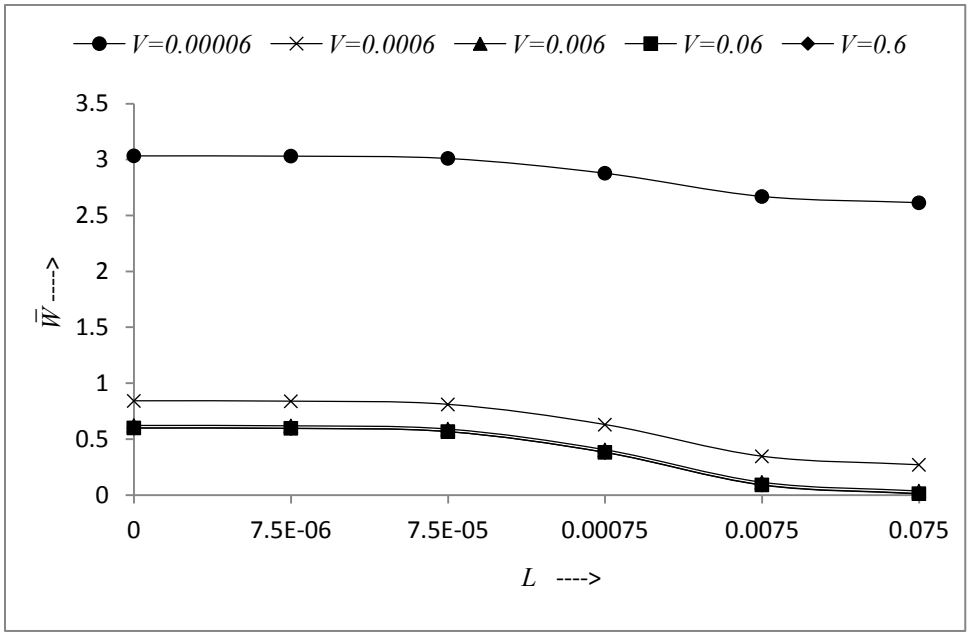

Figure 4.6 Values of $\bar{W}$ for various values of L versus V when $\beta = 4$, $K = 10^{13}$, $\varphi_r = \psi_r = 10^{-8}$ and $\Omega_l = 2$ for h_e and h_p

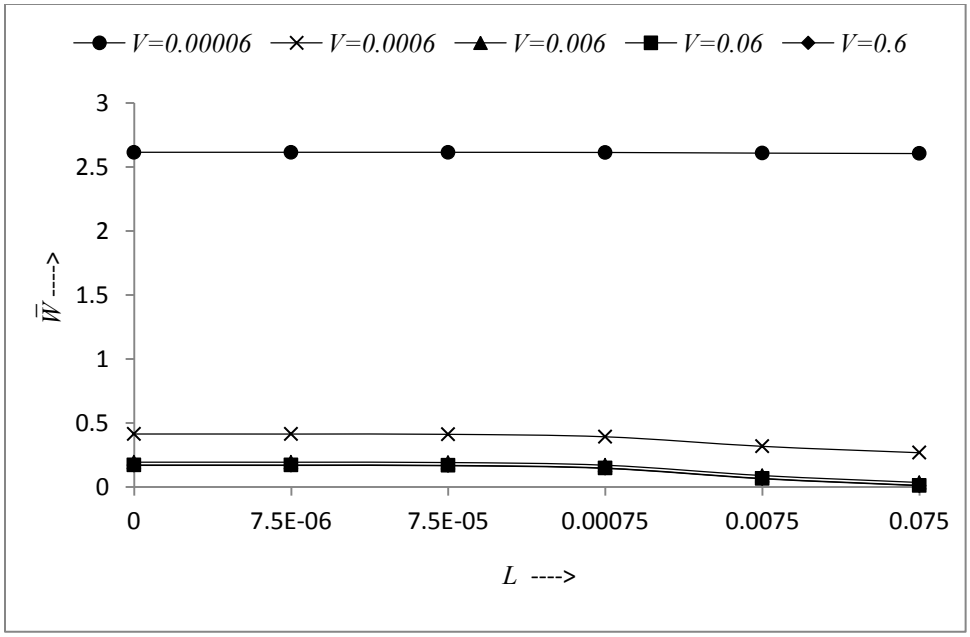

Figure 4.7 Values of $\bar{W}$ for various values of L versus V when $\beta = 4$, $K = 10^{13}$, $\varphi_r = \psi_r = 10^{-8}$ and $\Omega_l = 2$ for h_s

Figure 4.8 Values of $\bar{W}$ for various values of L versus β when $K = 10^{13}$, $V = 0.06$, $\varphi_r = \psi_r = 10^{-8}$ and $\Omega_l = 2$ for h_e

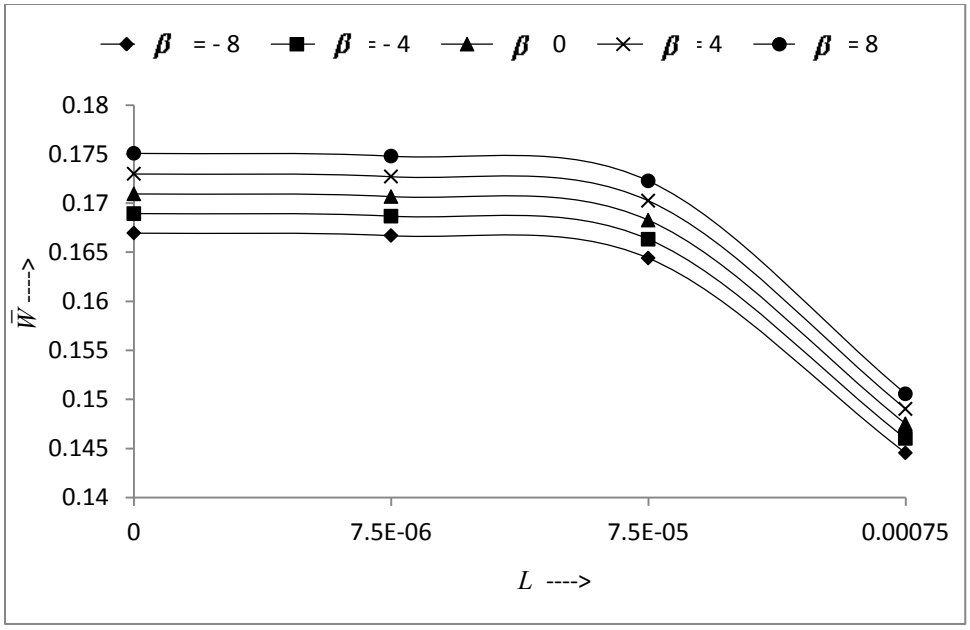

Figure 4.9 Values of $\bar{W}$ for various values of L versus β when $K = 10^{13}$, $V = 0.06$, $\varphi_r = \psi_r = 10^{-8}$ and $\Omega_l = 2$ for h_s

Figure 4.10 Comparative study of $\bar{W}$ for various values of L versus when $K = 10^{13}$, $V = 0.06$, $\varphi_r = \psi_r = 10^{-8}$, $\Omega_l = 2$ and $\beta = 4$ for h_e and h_s

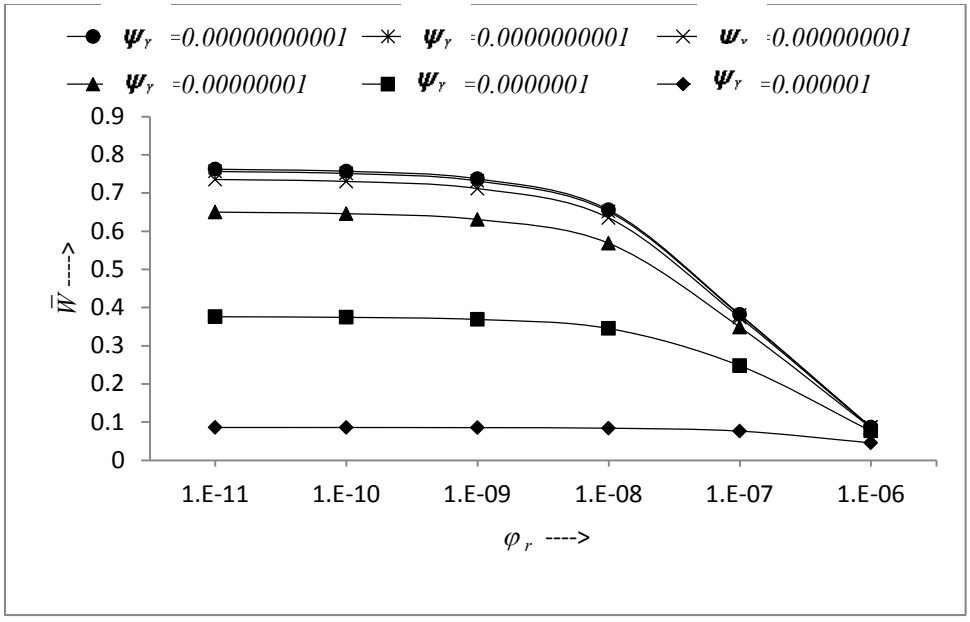

Figure 4.11 Values of $\bar{W}$ for various values of φ_r versus ψ_r when $\beta = 4$, $V = 0.06$, $l_1 = l_2 = 0.000075$, $K = 10^{13}$ and $\Omega_l = 2$ for h_e and h_p

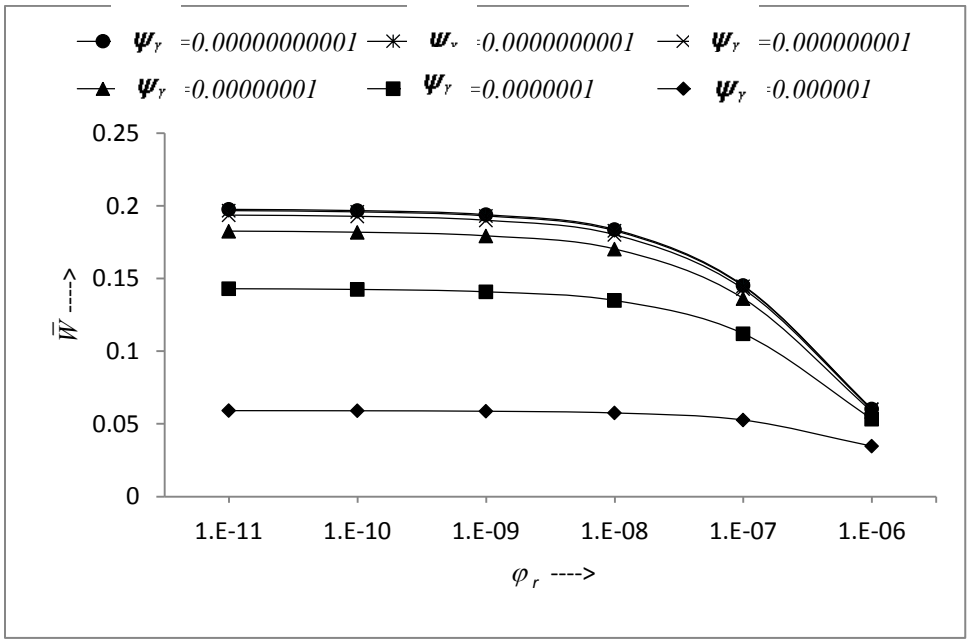

Figure 4.12 Values of $\bar{W}$ for various values of φ_r versus ψ_r when $\beta = 4$, $V = 0.06$, $l_1 = l_2 = 0.000075$, $K = 10^{13}$ and $\Omega_l = 2$ for h_s

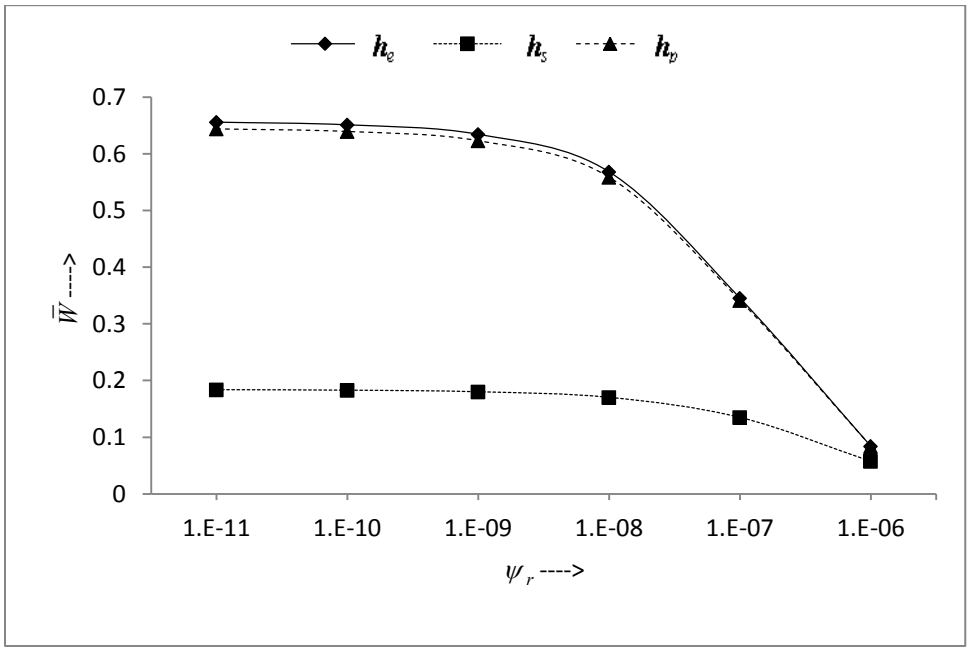

Figure 4.13 Comparative study of $\bar{W}$ for various values of ψ_r when $l_1 = l_2 = 0.000075$, $\beta = 4$, $V = 0.06$, $K = 10^{13}$, $\Omega_l = 2$ and $\varphi_r = 10^{-8}$ for h_e, h_s and h_p

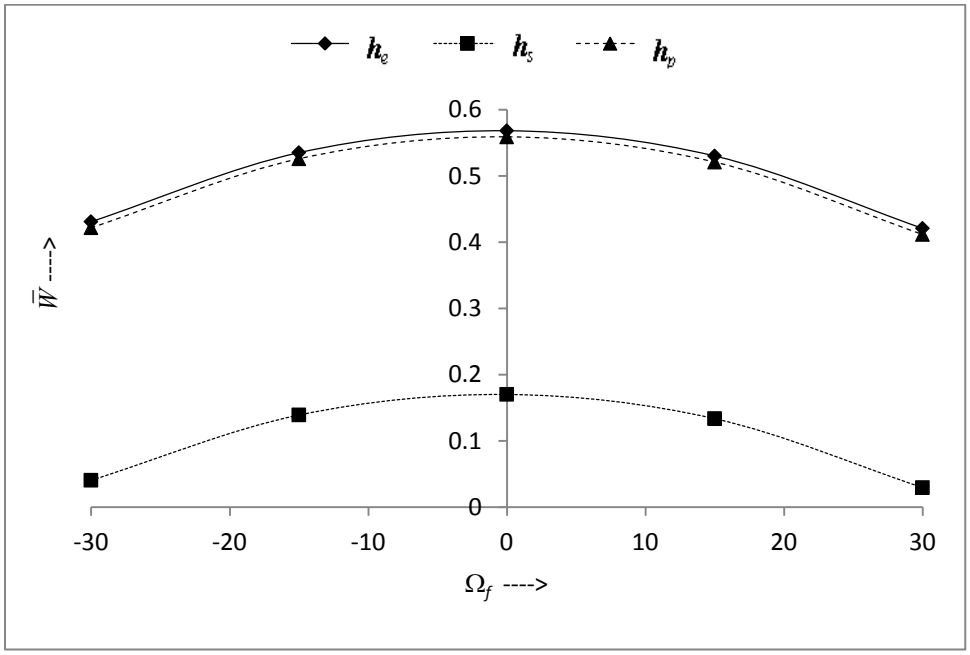

Figure 4.14 Comparative study of $\bar{W}$ for various values of Ω_f when $K = 10^{13}$, $\beta = 4$, $V = 0.06$, $l_1 = l_2 = 0.000075$ and $\varphi_r = \psi_r = 10^{-8}$ for h_e, h_s and h_p